Topological Defect Guided Order Evolution across the Nematic-Smectic Phase Transition

Sai-Bo Wu, Jin-Bing Wu, Hui-Min Cao, Yan-Qing Lu,[*] and Wei Hu[†]

National Laboratory of Solid State Microstructures, Key Laboratory of Intelligent Optical Sensing and Manipulation, College of Engineering and Applied Sciences, Nanjing University, Nanjing 210023, China

Topological defects usually emerge and vary during the phase transition of ordered systems. Their roles in thermodynamic order evolution keep being the frontier of modern condensed matter physics. Here, we study the generations of topological defects and their guidance on the order evolution during the phase transition of liquid crystals (LCs). With a given preset photopatterned alignment, two different types of topological defects are achieved depending on the thermodynamic process. Because of the memory effect of LC director field across the Nematic-Smectic (N-S) phase transition, a stable array of toric focal conic domains (TFCDs) and a frustrated one are generated in S phase, respectively. The frustrated one transfers to a metastable TFCD array with a smaller lattice constant, and further changes to a crossed-walls type N state due to the inheritance of orientational order. A free energy on temperature diagram and corresponding textures vividly describe the phase transition process and the roles of topological defects in the order evolution across the N-S phase transition. This Letter reveals the behaviors and mechanisms of topological defects on order evolution during phase transitions. It paves a way for investigating topological defect guided order evolution which is ubiquitous in soft matter and other ordered systems.

Topology, an unchanged property during continuous deformations in space, is intensively studied in modern condensed matter physics, including the quantum Hall effect [1], topological insulator [2], and topological superconductor [3]. The topological invariance endows corresponding systems with a protected symmetry that is rigorously defined by their topological characteristics. Symmetry breaking usually occurs during the phase transition of ordered systems, accompanied by the emergence and variation of topological defects. To date, the roles of topological defects in order evolution across phase transitions have long been an important topic of study, referring to Kosterlitz-Thouless phase transition [4], 2D melting [5], and cosmology in the laboratory [6]. Further exploring the behaviors and mechanisms of such defects in phase transitions with preprogrammed director fields will enrich our knowledge on condensed matters.

Liquid crystals (LCs) are known for their richness in topological defects and phases [7]. In the nematic phase (N), the rodlike LC molecules spontaneously orient along a dominant direction, referred to as the director. In equilibrium, point and line disclinations are generated due to the discontinuity of LC orientations. Besides, nonsingular defect walls, with directors either parallel or normal to the surface easy orientation axis, are involved at the border between two domains of opposite distortions. These topological defects are typically micrometer sized and optically anisotropic, thus they can be directly observed under a polarization optical microscope (POM). The generation and control of disclination lines are demonstrated via laterally shifting the alignment singularities on opposite substrates [8] or presetting the surface alignments [9]. Such disclination lines can be further manipulated actively by rewriting the unidirectional easy orientation on one substrate [10]. Compared to the abundant research on disclinations, defect walls are much less documented. They are of higher energy and are usually transferred from disclination lines under certain external fields [11]. Across the N-smectic (S) phase transition, the symmetry breaks in both rotational and translational dimensions. The system tends to carry on previously orientational order but slightly varies positionally to meet the new symmetric requirements. A one-dimensional positional order is established, and LC molecules arrange in parallel to form separate layers. As a result, dislocations arise instead of the above defect species existing in the N phase [12]. The evolution of point defects connecting water-LC-air interfaces [13], the variation of defects in LC confined by chemically patterned surfaces [14], the transformation of disclination lines for nanorod assembling within geometrical confinement [15], as well as the motions of point defects in spherical shells [16,17] and hyperbolic hedgehog defects in LC colloidal particles [18] have been studied. All above phenomena are mainly attributed to the divergences of both twist and bend elastic constants across the N-S phase transition. In contrast, the influence of topological defects on the order evolution across the N-S phase transition evolution has not yet been investigated.

In this Letter, a tetragonal lattice of radially aligned units and an opposite vertically aligned surface are adopted to

define the topological defects of LCs. Two different topologies are achieved via cooling from the isotropic (iso) state: a pure point defect array is generated in the N phase during a gentle cooling process, and unidirectional disclination lines arise in rapid cooling. These disclination lines transform to crossed walls after several thermal cycles across the N-S phase transition, leading to the emergence of the third stable (metastable) state at N phase. The Landau–de Gennes numerical modeling is utilized to reproduce the director distributions of the distinct states and clarify the transformation mechanism. After the N-S phase transition, the first and third cases induce two stable toric focal conic domains (TFCDs) arrays with different lattice constants. While the second one changes to unstable frustrated TFCDs. An energy-temperature diagram is plotted to vividly describe the phase transition process. The energy differences among the three N states are calculated. The inheritance of orientational order and topological invariance in order evolution can explain these transformations. This Letter focuses on the role of topological defects in the order evolution during phase transitions. It brings new phenomena to LCs and enriches the insight to soft matter and other ordered systems as well.

A hybrid cell with a gap $h = 8.8\ \mu m$ is adopted to provide an antagonistic boundary condition [see Fig. S1 in Supplemental Material (SM) [19]]. A thin PDMS layer covered superstrate gives vertical alignment, while the photoalignment agent SD1 [22] coated substrate gives planar anchoring. Figure 1(a) reveals a face-centered tetragonal lattice of alignment singularities recorded in SD1. The director field is depicted as

$$\alpha(x, y) = \sum_i s_i \arctan\left(\frac{y - y_{0i}}{x - x_{0i}}\right) + \alpha_{0i}, \quad (1)$$

where topological charge $s_i = \pm 1$, (x_{0i}, y_{0i}) are the coordinates of singularities, and α_{0i} is a constant initial orientation. Here, only two types are involved: ($s = +1, \alpha_0 = 0°$) and ($s = -1, \alpha_0 = 90°$), and the lattice constant $l = 20\ \mu m$. When the infiltrated 8CB is gently annealed ($-0.2\ °C/\min$) from the iso phase, LCs reorganize under the guidance of local alignment to form an ordered texture. The directors on the SD1 coated substrate follow the patterned planar alignment, while they turn to a uniform vertical alignment on the PDMS coated superstrate. A tetragonal lattice of Maltese crosses is observed under POM [Fig. 1(b)]. The sign of point defects (± 1) can be distinguished via checking the rotational direction of Maltese crosses compared to that of the polarizers. Different interference colors (cyan and magenta) are attributed to the distinct phase retardations caused by the spatially variable tilt angle of the LC director.

The LC director distribution is modeled according to the Landau–de Gennes theory (for the explicit forms and detailed parameter description, see SM [19]) and exhibited in Fig. 1(c). Considering the director variation in the z dimension, $+1$ point defects are divided into two distinct species: (1) center-converging (C) type (cyan), where the polar angle (the angle between the director and the z axis) $\theta > 90°$ and thus the director field converges toward the defect core; (2) center-diverging (D) type (magenta), where $\theta < 90°$ and the director field diverges from the defect core. For the -1 point defect, only one hyperbolic type exists, in
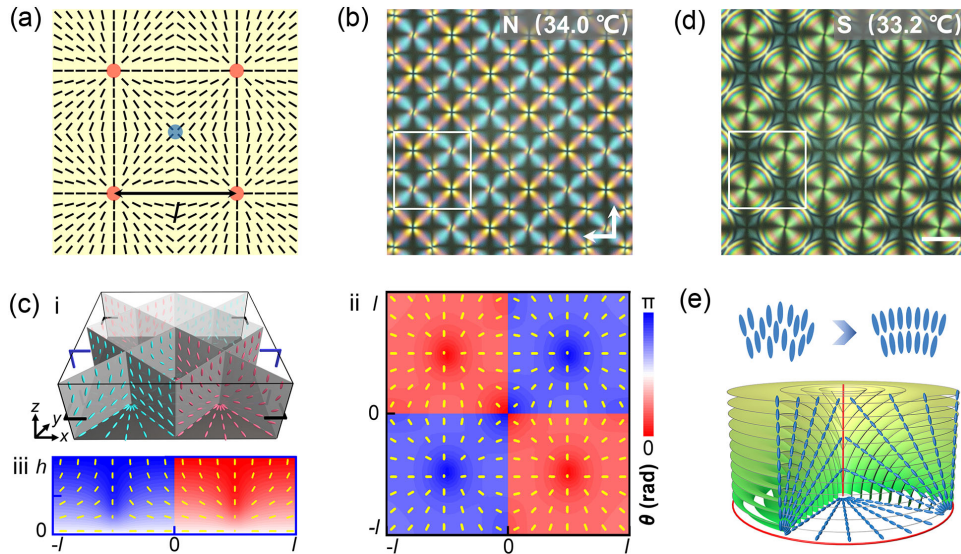

FIG. 1. (a) Lattice for alignment singularities of $s = +1$ (red dots) and -1 (blue dot). (b) POM image of the N phase texture at 34.0 °C. (c)(i) Three-dimensional (3D) director fields of the texture in (b); (c)(ii) and (c)(iii) reveal simulated director fields and calculated distributions of θ in marked sections. (d) POM image of the S phase texture at 33.2 °C. (e) Director field evolution across N-S phase transition, the layered configuration and director distribution corresponding to single TFCD in Fig. 1(d). The white arrows denote the directions of crossed polarizers. All scale bars indicate 20 μm.

which the above two cases coexist alternatively in two orthogonal planes. As shown in Fig. 1(c)(ii) and Fig. 1(c)(iii), the directors around the defect cores escape along the z dimension, facilitating the energy reduction of entire system [23]. The calculated director distribution is consistent with the interference color variation in the micrograph [Fig. 1(b)]. After the N-S phase transition, a tetragonal TFCDs array is formed [Fig. 1(d)]. Thanks to both the boundary constraint of the patterned substrate and the inheritance of the LC bulk elasticity, the orientational order of the LC director field can be roughly maintained across the phase transition in spite of thermal disturbance. The inheritance of orientational order, also referring to as the memory effect [24], reflects the balance among bulk energy, elastic energy, and anchoring energy. In each domain, LC layers are wrapped around a defect pair (red) of a straight line and a circle [Fig. 1(e)]. Because of the director-field-match requirement, TFCDs are always transformed from C-type point defects. Therefore, a tetragonal TFCDs array with a lattice constant of $\sqrt{2}l$ is obtained.

In a rapid cooling process ($-1\,°C/\min$), unidirectional disclination lines arise over the whole alignment region after temperature T decreases below the clearing point [Fig. 2(a)(i)]. In this case, the system energy cannot sufficiently release and thus choose another way to reduce the free energy F, i.e., decomposing integer defects into pairs of half-integer defects and forming disclination lines between adjacent $+1/2$ and $-1/2$ defects, accordingly [25]. The above discussion is further verified by the simulated director field [Figs. 2(a)(ii) and 2(a)(iii)]. The directors astride the disclination lines are discontinuous, which are converging (blue) and diverging (red), respectively. And the distance between adjacent disclination lines decreases with the increasing of the anchoring energy. When approaching the N-S phase transition point ($T_{N\text{-}S}$), the converging regions transform to focal conic domains (FCDs) with the eccentricity of elliptical defect e approaching 0, while the diverging regions transform to FCDs of high e [Fig. 2(b)]. Their connections induce many dislocations with the total Burgers vector $b_\varepsilon = 2ae$, where a is the long axis of the elliptical defect. Each dislocation carries an elastic energy of $\sim\sqrt{B\overline{k_{11}}}b_\varepsilon$, where B is the compression modulus and k_{11} is the splay elastic constant [26]. FCDs with high e are not stable and will transform to $e \to 0$ type configurations spontaneously. As a result, the smectic layers tend to form frustrated TFCDs [Fig. 2(c)].

The frustrated TFCDs still have many dislocations and do not match the constraint of radial alignments. Therefore, they are not thermodynamically stable. After slightly reheating ($0.1\,°C/\min$) to $T_{N\text{-}S}$, the mobility of LC under layer confinement as well as the suppression of twist and bend deformation at $T_{N\text{-}S}$ push dislocations to the unit boundaries [Fig. 2(d)]. When e decreases to zero, dislocations disappear. Therefore, TFCDs with $e = 0$ appear
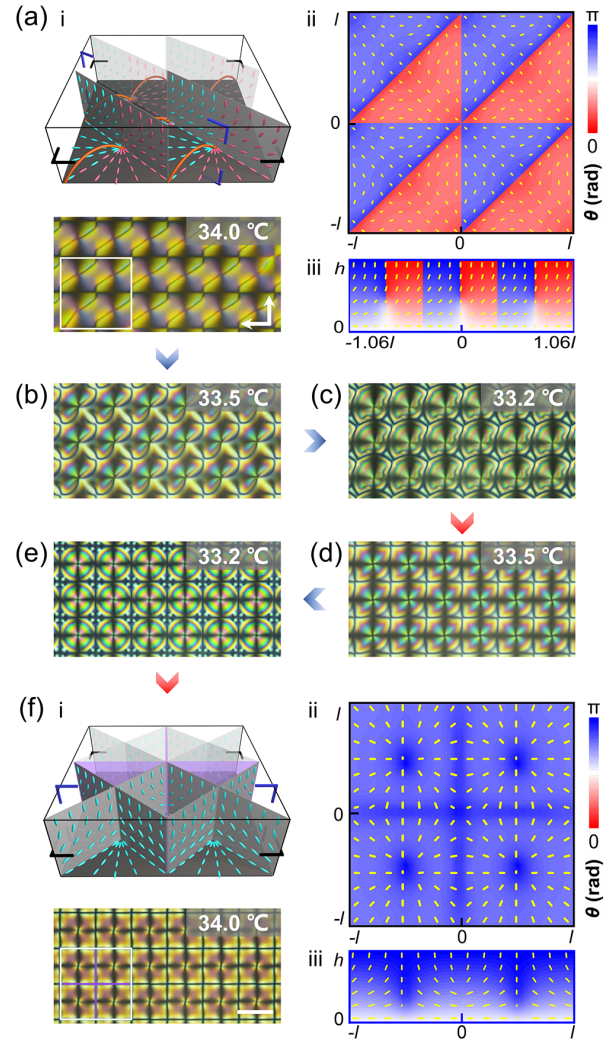

FIG. 2. (a)(i) 3D illustration and POM image of disclination lines (orange) in the N phase; (a)(ii) and (a)(iii) simulated director fields and calculated θ distributions of the marked sections. (b)–(e) Textural evolution in thermal cycling. (f)(i) 3D illustration and POM image of crossed walls (purple) in the N phase; (f)(ii) and (f)(iii) simulated director fields and calculated θ distributions of the marked sections. Blue and red arrows represent cooling and heating processes, respectively. The corresponding temperatures are labeled in the upper-right corners. All scale bars indicate 20 μm.

on each $+1$ singularity when T is below $T_{N\text{-}S}$ and a lattice constant of l is exhibited [Fig. 2(e)]. When TFCDs are reheated to the N phase, ordered crossed walls appear in the system instead of disclination lines [Fig. 2(f)(i)]. More detailed order evolution is provided as a movie in the SM [19]. As mentioned above, such an N state usually cannot exist without external fields. Here, the configuration is a direct inheritance of the TFCD director distribution. It is topologically protected and thus remains stable until transferring to the iso phase. The results are confirmed by simulations, where tetragonal C-type point defects with a constant l are separated by crossed walls [Figs. 2(f)(ii),
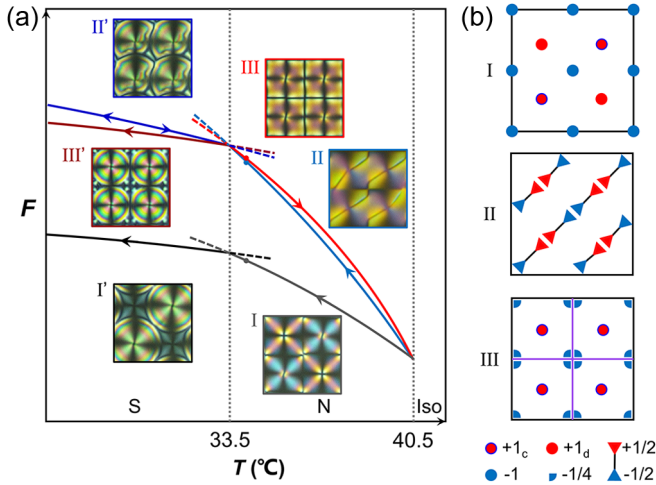
FIG. 3. (a) Dependencies of F on T for different states across $T_{N\text{-}S}$. (b) Topological analysis of the three different N states in (a).

FIG. 4. A 2D quasieutectic grows with different lattice constants ($\sqrt{2}l$ and l) and a coherent boundary in the (a) N and (b) S phases. The white arrows denote the directions of crossed polarizers. All scale bars indicate 20 μm.

2(f)(iii)]. It exhibits a distinguished director distribution compared to the gently cooling case (Fig. S2). Notably, when reheating to the iso phase and then cooling back to the N phase, disclination lines reappear, implying the lower energy of disclination lines compared to the crossed walls.

The above phenomena are summarized as the dependencies of F on T during the phase transition process in Fig. 3(a). The free energy landscape indicates that two different defect types (I, alternative ± 1 point defects and II, unidirectional disclination lines) are obtained via different energy releasing processes depending on the cooling rate. The numerical calculation reveals the Landau–de Gennes free energy difference $\Delta F_{\text{I-II}} = -0.256\ \mu\text{J}$ at 34 °C, suggesting that I is more stable than II (gray and blue dots, respectively). When $T < T_{N\text{-}S}$, TFCDs with lattice constants of $\sqrt{2}l$ (I′) and frustrated TFCDs (II′) arise due to the memory effect of director distribution across the $N\text{-}S$ phase transition. Compared to I′, II′ exhibits many dislocations and is not at thermodynamic equilibrium. It tends to eliminate these dislocations to minimize F during thermal cycling across the $T_{N\text{-}S}$. This pushes II′ to III′ (tetragonal TFCDs with lattice constant of l) transformation. Obviously, III′ is more stable than II′. When reheating to the N phase, III′ changes to III (crossed walls). The numerical calculation gives $\Delta F_{\text{II-III}} = -0.01\ \mu\text{J}$ at 34 °C, indicating II is more stable than III (blue and red dots, respectively). This is why III cannot be transformed from the iso phase directly.

Simulation indicates that the above multistate can be observed in the common range of anchoring energy (10^{-5}–$10^{-3}\ \text{J/m}^2$). Bulk energy also influences the defect transformation. Simulations and experiments suggest the robustness of transformations among the above states within wide ranges of h and l. Topological analysis helps us to better understand the above process. The topology of
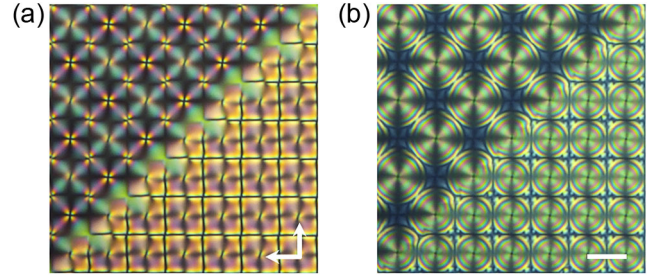
three different N states is shown in Fig. 3(b). The topology can be depicted by a sum of all defect types within a single unit. For the unit of state I, there are one $+1_C$ (red dot with blue outline) or $+1_D$ (red dot) point defect (equal in topology) in the center and four -1 (blue dot) point defects at the corners that are shared by the other three neighboring units. Therefore, the topology can be depicted as $\{+1; (-1) \times 1/4 \times 4\}$. Similarly, state II is depicted as $\{(-1/2 \sim +1/2) \times 2\}$, which means that each unit has two disclination lines connecting the adjacent $+1/2$ (red triangle) and $-1/2$ (blue triangle) defects. State III is depicted as $\{+1; -1/4 \times 4; 0\}$, which means each unit contains one $+1_C$ point defect in the center, four $-1/4$ (blue quarter disk) point defects at the corners, and crossed walls, which are equivalent to uniform configurations in topology. The topological invariance requirement restricts the direct transformation among these three different states. We find that different topological defect species evolve along separate paths during the $N\text{-}S$ phase transition: $+1_c$ point defects become TFCDs; $+1_d$ point defects change to domains with positive Gauss curvatures alternatively embedded into the TFCD lattice; $\pm 1/2$ disclination lines are transformed into unstable dislocations, and further turn to crossed walls in the N phase after thermal cycling.

Notably, states I and III can coexist in the form of quasieutectic in the N phase at a proper cooling speed (here, 0.5 °C/ min). As exhibited in Fig. 4, state I, state III and their corresponding TFCDs arrange on top-left and bottom-right, respectively. They are divided by a diagonal boundary along 45° where both lattices match each other strictly.

The generation of topological defects and their guidance on the order evolution of LC across $T_{N\text{-}S}$ are investigated. Distinct topological defects are generated with a same alignment condition via different thermodynamic processes. The director field simulations and free energy calculations, as well as corresponding textures indicate topological defects play vital roles in order evolution across the $N\text{-}S$ phase transition. The LC director field is inherited across the phase transitions. The topological protection leads to two metastable N states in addition to the stable

N state with alternative ± 1 point defects, especially making the crossed-wall type N state stable even without external field applied. This Letter provides new insight on the mechanism of LC topological defects guided order evolution across the phase transitions under patterned alignment, different from those previously reported in homogeneous environments. New defect transformation and metastable textures are brought to LCs, which are further explained by frustration evolution and topological invariance. The emergence of novel phenomena may enrich the knowledge on self-organized ordered systems and pave the way for advanced applications of defects.

---

*Corresponding author.
yqlu@nju.edu.cn
†Corresponding author.
huwei@nju.edu.cn

[1] D. J. Thouless, M. Kohmoto, M. P. Nightingale, and M. den Nijs, Phys. Rev. Lett. **49,** 405 (1982).

[2] J. E. Moore and L. Balents, Phys. Rev. B **75,** 121306(R) (2007).

[3] A. P. Schnyder, S. Ryu, A. Furusaki, and A. W. W. Ludwig, Phys. Rev. B **78,** 195125 (2008).

[4] M. A. Bates and D. Frenkel, J. Chem. Phys. **112,** 10034 (2000).

[5] S. C. Kapfer and W. Krauth, Phys. Rev. Lett. **114,** 035702 (2015).

[6] I. Chuang, R. Durrer, N. Turok, and B. Yurke, Science **251,** 1336 (1991).

[7] P. G. de Gennes and J. Prost, *Physics of Liquid Crystals* (Oxford University Press, New York, 1993).

[8] H. Yoshida, K. Asakura, J. Fukuda, and M. Ozaki, Nat. Commun. **6,** 7180 (2015).

[9] Y. B. Guo, M. Jiang, S. Afghah, C. H. Peng, R. L. B. Selinger, O. D. Lavrentovich, and Q. H. Wei, Adv. Opt. Mater. **9,** 2100181 (2021).

[10] J. H. Jiang, K. Ranabhat, X. Y. Wang, H. Richb, R. Zhang, and C. H. Peng, Proc. Natl. Acad. Sci. U.S.A. **119,** e2122226119 (2022).

[11] T. Ouchi, K. Imamura, K. Sunami, H. Yoshida, and M. Ozaki, Phys. Rev. Lett. **123,** 097801 (2019).

[12] H. Aharoni, T. Machon, and R. D. Kamien, Phys. Rev. Lett. **118,** 257801 (2017).

[13] M. J. Gim, D. A. Beller, and D. K. Yoon, Nat. Commun. **8,** 15453 (2017).

[14] T. Pawale, S. Z Yi, X. W. Wang, R. Zhang, and X. Li, Soft Matter **18,** 5939 (2022).

[15] E. Lee, Y. Xia, R. C. Ferrier Jr, H. N. Kim, M. A. Gharbi, K. J. Stebe, R. D. Kamien, R. J. Composto, and S. Yang, Adv. Mater. **28,** 2731 (2016).

[16] H. L. Liang, S. Schymura, P. Rudquist, and J. Lagerwall, Phys. Rev. Lett. **106,** 247801 (2011).

[17] T. Lopez-Leon, A. Fernandez-Nieves, M. Nobili, and C. Blanc, Phys. Rev. Lett. **106,** 247802 (2011).

[18] K. P. Zuhail, P. Sathyanarayana, D. Seč, S. Čopar, M. Škarabot, I. Muševič, and S. Dhara, Phys. Rev. E **91,** 030501(R) (2015).

[19] See Supplemental Material at http://link.aps.org/supplemental/10.1103/PhysRevLett.130.078101 for the detailed description of numerical modeling and parameters, the director field simulation for three different N states, a movie for the more detailed order evolution in phase transition processes, which includes Refs. [20–21].

[20] M. Ravnik and S. Zumer, Liq. Crys. **36,** 1201 (2009).

[21] H. Akiyama, T. Kawara, H. Takada, H. Takatsu, V. Chigrinov, E. Prudnikova, V. Kozenkov, and H. Kwok, Liq. Crys. **29,** 1321 (2002).

[22] M. Schadt, K. Schmitt, V. Kozinkov, and V. Chigrinov, Jpn. J. Appl. Phys. **31,** 2155 (1992).

[23] C. Chiccoli, I. Feruli, O. D. Lavrentovich, P. Pasini, S. V. Shiyanovskii, and C. Zannoni, Phys. Rev. E **66,** 030701(R) (2002).

[24] A. Suh, M. J. Gim, D. Beller, and D. K. Yoon, Soft Matter **15,** 5835 (2019).

[25] B. S. Murray, R. A. Pelcovits, and C. Rosenblatt, Phys. Rev. E **90,** 052501 (2014).

[26] M. Kleman and O. D. Lavrentovich, Phys. Rev. E **61,** 1574 (2000).